Journal of Sustainable Development of Energy, Water and Environment Systems

http://www.sdewes.org/jsdewes

Year 2026, Volume 14, Issue 3, 1140725

Original Research Article

Investigation of Process Feasibility and Mechanical Performance of *Prosopis Juliflora* Biobased Residue Materials for Additive Manufacturing

Mihreteab Kidanemariam Gebregewergs*[1,2], James Wamai Mwangi[3], Kabini Karanja[3], Monnamme Tlotleng[4,5]

[1]Department of Mechanical Engineering, Pan African University Institute for Basic Sciences, Technology, and Innovation (PAUSTI), Nairobi, Kenya

[2]Raya University, Maichew, Ethiopia

[3]Department of Mechatronic Engineering, Jomo Kenyatta University of Agriculture and Technology (JKUAT), Nairobi, Kenya

[4]Instruments Research and Development Group, Measurement and Control Division, Council for Mineral Technology (MINTEK), Randburg, Johannesburg, 2194, South Africa

[5]Materials Science Innovation and Modelling Research Group, North-West University, Mahikeng, Mmabatho 2745, South Africa

e-mail: mihreteabkidanemariam@rayu.edu.et, jwamai@jkuat.ac.ke, kkabini@eng.jkuat.ac.ke, MonnammeT@mintek.co.za

Cite as: Gebregewergs, M. K., Mwangi, J. W., Karanja, K., Tlotleng, M., Investigation of Process Feasibility and Mechanical Performance of Prosopis Juliflora Biobased Residue Materials for Additive Manufacturing, J.sustain. dev. energy water environ. syst., 14(3), 1140725, 2026, DOI: https://doi.org/10.13044/j.sdewes.d14.0725

ABSTRACT

Biobased residues from agriculturee and invasive plants can be used as cost-effective, sustainable alternative materials for additive manufacturing. This study investigates the feasibility of using *Prosopis juliflora*, an invasive and abundant species, as a feedstock for binder jetting and paste extrusion three-dimensional printing. Powders derived from *Prosopis juliflora* leaf, stem, and pod residues were characterised, and carboxymethyl cellulose was used as a binder in different formulations. Leaf and stem powders exhibited suitable powder properties, with stable powder-bed formation during binder jetting. In contrast, pods were sticky and tended to agglomerate, limiting their use in this process. Paste extrusion manufactured stable components for all fractions except at high binder ratios for pod-based materials. Mechanical testing showed maximum compressive strengths of 6.74 MPa, 10.17 MPa, and 4.64 MPa, and flexural strengths of 4.94 MPa, 13.45 MPa, and 9.44 MPa for leaf, stem, and pod samples, respectively. These findings demonstrate the potential of *Prosopis juliflora* residues as sustainable materials for additive manufacturing applications.

KEYWORDS

P. juliflora, Biobased material, Feasibility, Mechanical performance, Additive manufacturing.

INTRODUCTION

The development of new materials has been a focus of technological advancement and industrial growth, serving as a source of innovation that enhances manufacturing processes and product performance [1]. In recent decades, additive manufacturing (AM) or three-dimensional (3D) printing has created structures by adding material layer by layer from a Computer-Aided Design (CAD) model according to the desired design, and has grown into a revolutionary fabrication technique [2]. AM is increasingly recognised as a more sustainable

* Corresponding author

manufacturing method than conventional subtractive processes, enabling shorter design cycles and greater material utilisation [3], [4]. The latest progress demonstrates that combining computational optimisation methods with AM techniques, such as hybrid AM systems driven by AI [5] and machine-learning-assisted parameter control [6], can improve mechanical performance, minimise defects, and significantly enhance production efficiency. This kind of development indicates that AM has been moving towards highly intelligent, optimised manufacturing systems. Despite this technological advancement, most commercially available AM materials are petroleum-based polymers, energy-intensive metals, or synthetic composites that are energy-intensive, have limited sustainability, and impose environmental burdens.

There has been growing interest in recent studies to use biobased materials as AM feedstocks, driven by the need to reduce dependence on non-renewable, energy-intensive feed materials. Sekula *et al*. [7], using extrusion, High-Speed Sintering (HSS), and selective laser sintering (SLS), processed a biodegradable composite material consisting of a cellulose acetate propionate and microcrystalline cellulose for high-voltage electrical insulators and concluded that although the mechanical properties of the processed biopolymer were below industrial acceptance, the composite materials remain promising for sustainable manufacturing of high-voltage cellulose insulators. Complementary works further emphasise that developing low-cost waste-derived feedstocks can significantly improve material utilisation rates and support circular economy principles in AM [8].

The application of biobased materials in AM, however, is difficult due to their irregular particle morphology, poor flowability, and moisture sensitivity, especially in powder-based processes. Among the several AM techniques, binder jetting (BJT) and paste extrusion (MEX) are showing potential for utilising agricultural byproducts and invasive plant species as viable and low-cost alternative feed materials. BJT offers several advantages, including simple operation, high printing speed, good powder bed capacity, and the ability to tailor the microstructure and properties of the final part without requiring melting or extrusion [9], [10]. In contrast, MEX requires careful control of binder content, paste viscosity, extrusion rate, and drying behaviour, as these elements have a profound impact on the dimensional stability and mechanical performance of printed components [11].

Previous studies have investigated the use of biobased and waste-derived materials in both BJT and MEX processes. For instance, Micke *et al*. [12] investigated the use of water hyacinth, an invasive aquatic species in Kenya, as a feedstock in BJT and achieved parts with a compressive strength of 0.47 N/mm^2. Similarly, Khan *et al*. [13] examined waste algae powder in binder jetting, reporting a green density of 0.70 g/cm^3 and compressive strength of 1.3 N/mm^2. These findings support the feasibility of utilising biobased residues in powder-based AM processes. In extrusion-based processes, Hussein *et al*. [14] explored the strength of printed parts composed of rice husk and an alginate binder through a modified MEX 3D printer. They noted that the binder ratio and moisture content were significant factors that affect mechanical strength and dimensional accuracy. Andanje *et al*. [15] used recycled High-Density Polyethylene (rHDPE) and rice husks as composite filament feedstock for the development of an extrusion-based 3D printing technology. The research conducted by Bah *et al.* [16] produced sustainable composite filaments using rHDPE and cactus powder for Fused Filament Fabrication (FFF), demonstrating the applicability of agricultural residues in extrusion-based techniques.

In addition to agricultural waste, utilising invasive plant species in AM has gained attention. *Prosopis juliflora* (*P. juliflora*), being both abundant and invasive, shows great promise for transformation into valuable materials. This trend would not only facilitate efficient control of their spread but also yield economic and environmental benefits. Materialistically, *P. juliflora* is a fibrous material consisting mainly of cellulose (30–40%), hemicellulose (25–30%), and lignin (20–25%) along with other minor extractives and ash [17].

Recent studies have examined the utilisation of *P. juliflora* using different methods. In the field of structural materials, Santhosh *et al*. [17] reported that adding rice husk to *P.*

juliflora-epoxy composites improved the mechanical performance by approximately 45% relative to the unmodified composites. Subbiah *et al*. [18] synthesised a hybrid composite comprising *P. juliflora* and *Phoenix sylvestris* fibres, glass fibres, and epoxy resin using the hand lay-up process, demonstrating improved fibre-matrix bonding strength post-alkali treatment. Apart from the structural purposes, Debella *et al*. [19] found that *P. juliflora* could be utilised as a promising material for biodiesel production, producing methyl esters which met the American Society for Testing and Materials (ASTM) biodiesel fuel standards. Furthermore, Rao *et al*. [20] produced a heterogeneous biochar-based catalyst using pyrolysis of *P. juliflora* biomass waste for biodiesel production. However, previous studies have focused on conventional processes, such as composite fabrication and biodiesel production. To the authors' knowledge, no prior study has evaluated the printability of different *P. juliflora* plant fractions (leaves, stems, and pods) across different AM techniques.

The present study addresses this gap by evaluating the suitability of *P. juliflora* residues as filler materials in BJT and MEX. The choice of leaf, stem, and pod fractions was motivated by the need to utilise the whole plant efficiently by processing each fraction separately, thereby enhancing material efficiency during biomass conversion. Each fraction exhibits unique morphological, flow, and rheological properties, as well as binder interactions, which greatly impact AM processability and final product performance [21].

Feasibility is assessed using indicators such as powder flowability, particle size distribution (PSD), morphology, powder-bed formation (for BJT), extrusion stability, and dimensional retention (for MEX). Since the present work focuses on preliminary powder characterisation and powder-bed formation in BJT, detailed mechanical testing of binder-jetted parts is reserved for ongoing research involving experimental design and optimisation. Mechanical evaluation in this study, therefore, focuses on paste-extruded components. The specific objectives of this study are to: (i) characterise the physical and flow properties of the *P. juliflora* powders for BJT, (ii) evaluate the printability of the residual materials under binder jetting conditions, (iii) develop and assess printable pastes to use in extrusion-based printing, and (iv) evaluate the mechanical properties of paste-extruded parts under varying volumetric flow rates and binder ratios.

MATERIALS AND METHODS

This section presents the materials used and the experimental methods employed in the research work. It includes details on the collection and preprocessing of *P. juliflora* residues, powder preparation and characterisation, selection of process parameters, and mechanical testing of 3D printed components.

Material Description and Sample Collection

The *P. juliflora* species, originally from Central and South America, was intentionally brought to dry and semi-dry areas to support land recovery and provide fuelwood [22], [23]. It has since spread widely across Africa, Asia, the Middle East, and parts of Australia, where it is now often seen as an invasive species that brings about serious ecological and socio-economic issues [22]. For example, it forms dense thickets that reduce biodiversity, degrade grazing land, and lower water tables in affected regions [24]. However, despite these negative effects, its abundance offers a significant opportunity to develop sustainable materials and utilise them in new manufacturing technologies. Given its widespread presence, especially in arid and semi-arid regions, *P. juliflora* was chosen for this study as a source of biobased material. **Figure 1** shows that the species has established dense stands in countries including Kenya, Ethiopia, Sudan, India, Pakistan, Australia, Brazil, Mexico, and the United Arab Emirates [25].

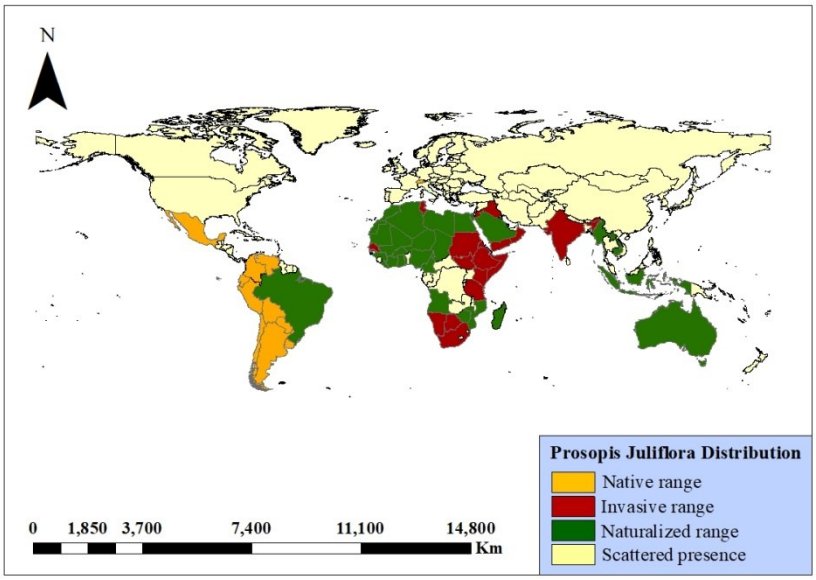


Figure 1. Global distribution areas of the Prosopis juliflora plant [25]

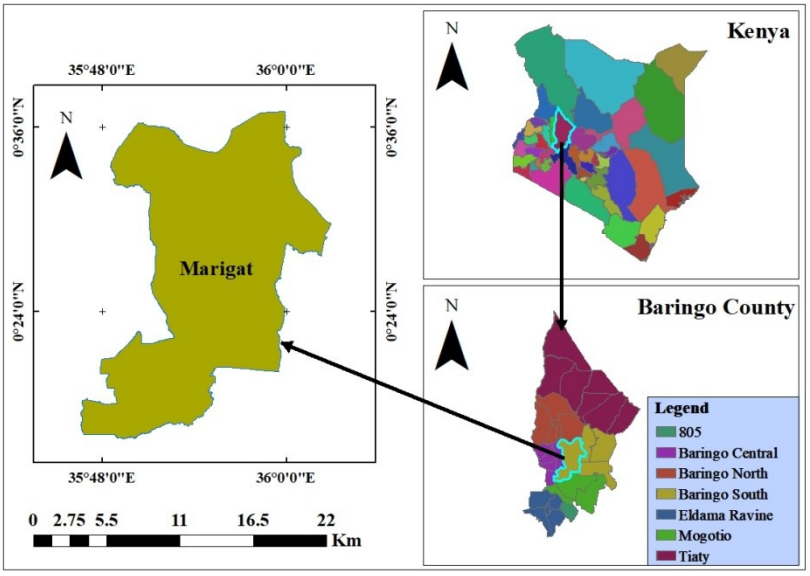


Figure 2. Location of the study area in Marigat, Baringo County, Kenya

For experimental consistency, the raw material was collected in Marigat, Baringo County, Kenya, a location known for its high density of mature *P. juliflora* stands [26]. For clarity, Figure 2 shows the map of the Marigat area from which the samples used in this study were collected. The biobased residues used for the AM processes were derived from the leaves, stems, and pods of the collected plants. Processing distinct parts helps observe variations in powder properties that are crucial for effective powder spreading in BJT and paste behaviour in MEX processes.

Material Preprocessing

The freshly obtained *P. juliflora* residues were cleaned and washed to remove dust, dirt, and organic materials. All materials were dried in a closed solar dryer for seven days to mitigate environmental factors such as moisture. The daily average temperature and relative humidity inside the solar dryer were approximately 40 $\pm$ 5 °C and 50.7 $\pm$ 5%, respectively. Although the average temperature was moderate, peak mid-day temperatures of ~60 °C combined with low relative humidity (~22%), provided complete moisture removal without requiring external energy input. Precrushing of residues was performed using a hammer mill

with a 1.5 kW power rating and an approximate throughput of 15 kg/h to reduce the materials into smaller particles for subsequent milling. Fine powders suitable for 3D printing were then produced by ball milling (4 kW), obtaining approximately 6 kg of powder in 2 hours. **Figure 3** illustrates the equipment used for drying and grinding in the study. These procedures resulted in a suitable fine powder for the BJT and MEX processes.

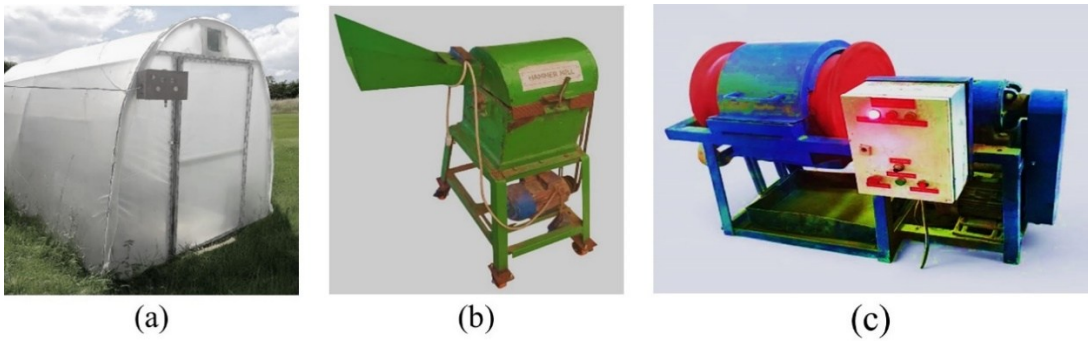


Figure 3. Equipment used for drying and grinding: solar dryer (a), hammer mill (b), and ball mill (c)

The overall preprocessing of *P. juliflora* residue materials into a range of printable powders was carried out at Jomo Kenyatta University of Agriculture and Technology (JKUAT), Kenya, as shown in **Figure 4**, with the corresponding flow diagram outlined in **Figure 5**.

The energy required for the preprocessing operation was estimated based on the power ratings of the machines used and the time required to process the materials, and compared with literature values for conventional lignocellulosic biomass grinding. In this respect, the drying process was powered by solar energy, so the external energy requirement was insignificant. Energy requirements for mechanical grinding have been reported to range from 0.1–0.5 kWh/kg and 0.5–2 kWh/kg for hammer milling and ball milling, respectively. The reported values align with those in the literature **[27]**, indicating lower energy demand than in conventional thermal drying and high-energy milling.

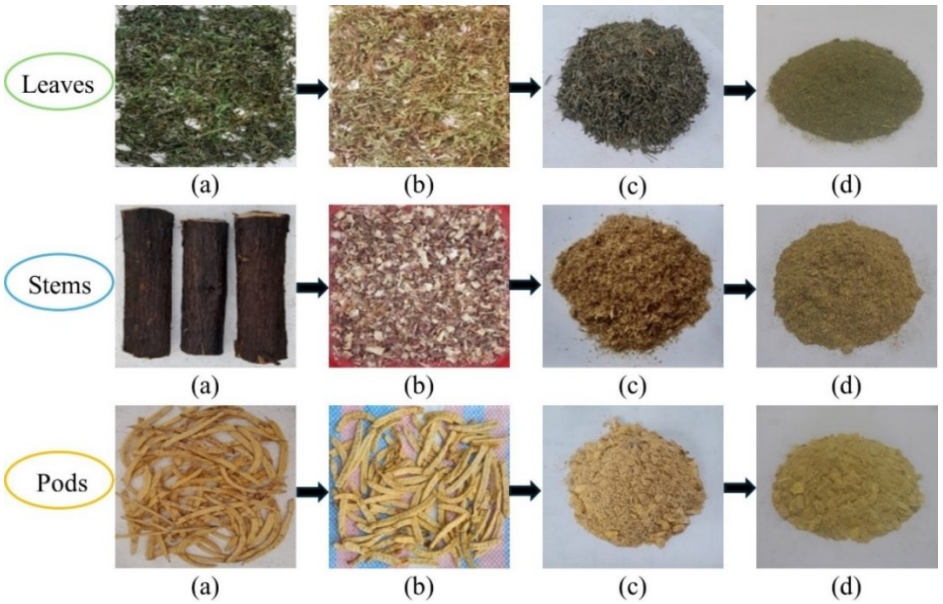


Figure 4. Preprocessing steps of residue materials: freshly harvested and cleaned (a), after complete drying (b), after crushing (c), and after ball milling (d)

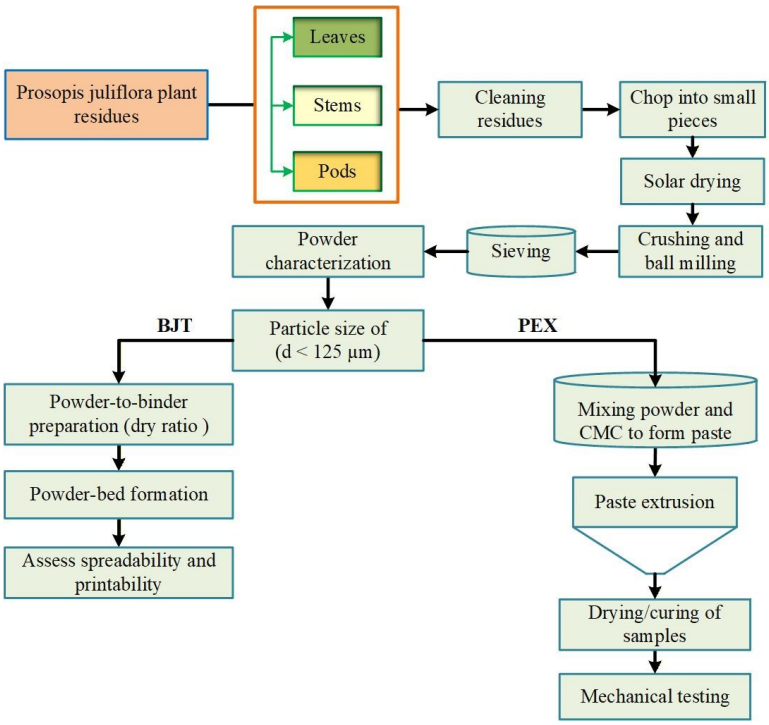


Figure 5. Flow diagram for the preparation, printing, and testing of residue powder materials

Powder Characterisation

The physical and morphological characteristics of *P. juliflora* powders were studied using a standard procedure at JKUAT in Kenya. All measurements were carried out in triplicate, and average values are reported. Moisture content was determined using a KERN DAB moisture analyser [28], as illustrated in Figure 6a. The bulk density of powders was measured according to DIN ISO 60 "Art. No. 5346800" [29], [30]. In every bulk density measurement, the mass of the empty density cup was first measured. Powder was then added to the funnel through the funnel opening, as shown in Figure 6b, which is narrower than the funnel. The powder is fed through gravity, filling the measuring cylinder under the funnel, forming a cone, and overflowing. The cone was carefully scraped off using a spatula, and the weighing cylinder holding the powder was weighed as shown in Figure 6c.

To determine the bulk density for each measurement, the net powder mass in the cylinder was divided by the cylinder's volume (V = 100 cm^3). Tap density was measured using a JEL STAV II tap density tester (J. ENGELSMANN AG) after a predefined number of taps until volume stabilisation [31], as shown in Figure 6.

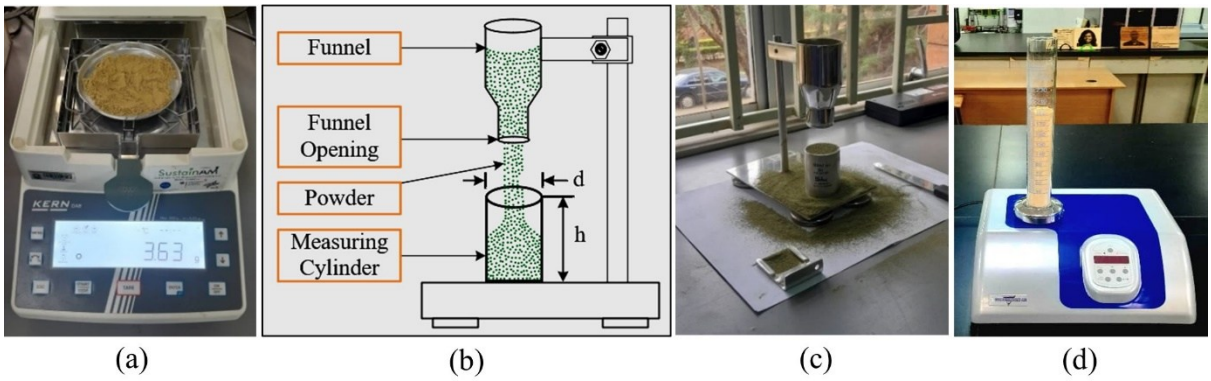


Figure 6. Measuring apparatus: measurement of moisture content (a), Hall flowmeter setup (b), measurement of bulk density (c), and measurement of tap density (d)

The flow properties and packing behaviour of the powder were evaluated using the Carr Index (*CI*) and Hausner Ratio (*HR*), calculated from bulk density (ρ_{bulk}) and tap density (ρ_{tap}) as per eq. (1) and eq. (2), respectively [32]:

$$CI = \left(\frac{\rho_{tap} - \rho_{bulk}}{\rho_{tap}}\right) \times 100 \quad [\%] \tag{1}$$

$$HR = \frac{\rho_{tap}}{\rho_{bulk}} \tag{2}$$

Table 1 shows a summary of the classification of flow behaviours of *P. juliflora* powder fractions, based on the criteria proposed by powder-process.net [33]. The powder fractions were morphologically characterised using a scanning electron microscope (SEM) [34] with a secondary electron detector (SED). All images were taken using high vacuum at an accelerating voltage of 15 kV, and a working distance of ~20 mm. Samples were mounted on conductive stubs and sputter-coated to avoid charging.

Table 1. Classification of powder flowability based on CI and HR for BJT 3D printing

Flow character	Carr index [%]	Hausner Ratio	Numerical rating [1–5]	Description of powder suitability
Extremely poor	> 38	> 1.60	1	Unsuitable for BJT
Very poor	32–37	1.46–1.59	2	Significant limitations
Poor	26–31	1.35–1.45	2–3	Marginally suitable
Passable	21–25	1.26–1.34	3	Acceptable for experimental use
Fair	16–20	1.19–1.25	3–4	Usable
Good	11–15	1.12–1.18	4	Suitable for printing
Excellent	< 10	1.00–1.11	5	Optimal flow for BJT

SEM micrographs were obtained at different magnifications to provide a clear observation of particle shapes and surface textures. These observations provided essential insights into particle morphology, which influences powder dispersion and spreading in the BJT process. The d < 125 µm particle size, common to all materials, was selected for PSD analysis and printing due to its balanced flow properties and preliminary trials of spreading and layer formation. PSD was conducted using a laser diffraction particle size analyser (model: SALD-2300, No. I563258E0704).

Powder-Bed Formation in Binder Jetting

A preliminary evaluation of powder behaviour was conducted using printability trials with Zcorporation's "ZPrinter 310" 3D printer, as shown in Figure 7, at the Sustain AM laboratory in JKUAT. Small amounts of powder were loaded into the feed bed, and the spreading function was activated several times to spread a thin layer of powder from the feed bed onto the build bed. The resulting powder layers were then qualitatively analysed for their uniformity, packing stability, and tendency to clump or segregate [35].

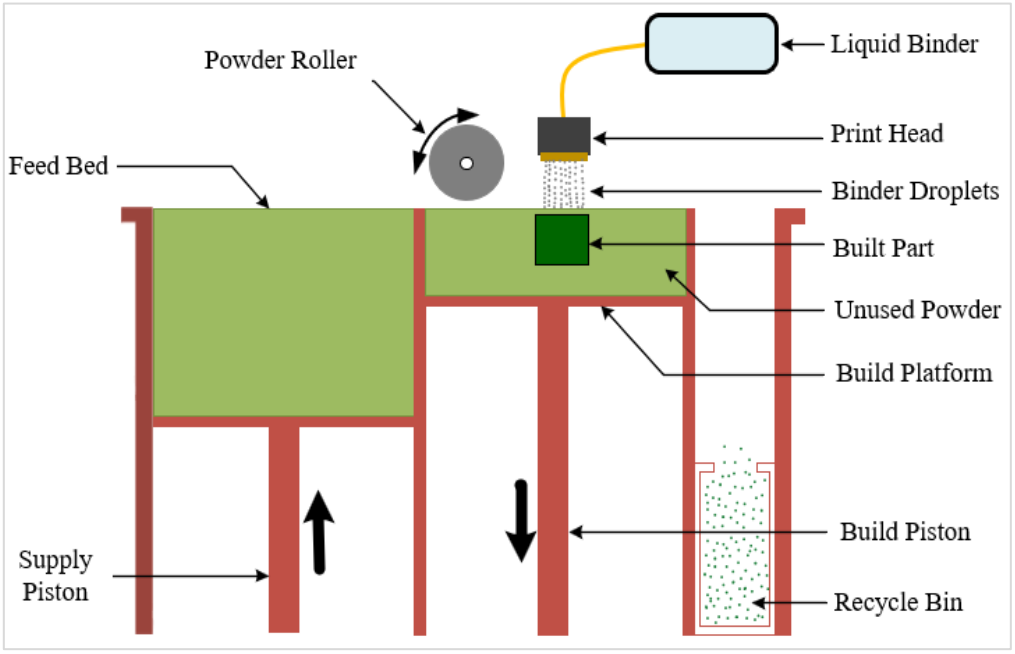


Figure 7. Schematic of the binder jetting using the "ZPrinter 310" 3D printer

To further assess buildability, cubic specimens (20×20×20 mm) were designed in SolidWorks 2019 and printed with a layer thickness of 0.1 mm, approximately twice the mean particle size [13], a binder saturation of 120%, and a powder-to-binder (P/B) ratio of 85/15 (15 wt.% of binder) to balance particle adhesion and material efficiency [36]. Carboxymethyl cellulose (CMC) [37], [38] was utilised as a solid binder. The liquid binder consisting of 100 mL isopropanol, 50 mL glycerin, 10 mL liquid SDS, and distilled water (total volume of 1 L) was also used for printing the parts. The printability of powders and the dimensional consistency of the green parts were visually analysed.

Paste Printability and Sample Preparation Using Paste Extrusion

This subsection briefly presents the procedures adopted in the study to ensure the reliability and repeatability of paste extrusion and printing tests.

Paste formulation and preparation. Because *P. juliflora* powders are highly absorbent and sticky, paste formulations were prepared by mixing the powder fractions with a water-soluble CMC binder. Two P/B ratios, by weight per cent, i.e., 85/15 (15 wt.% CMC) and 70/30 (30 wt.% CMC), were investigated for each material fraction. These ratios were selected to represent low and high binder contents within a practical processing range to assess the effects of binder content on paste flowability, filament stability, and mechanical performance. Dry powders were first homogenised to ensure uniform binder distribution. Water was then gradually added during manual mixing to obtain a workable paste capable of continuous extrusion. Depending on the formulation and nature of the material, moisture content ranged from 54% to 68% by total weight. The moisture content was not treated as an independent process parameter; rather, it was adjusted only to achieve extrudable consistency. Preliminary printability tests were conducted to assess whether the paste could be easily extruded and form stable, continuous layers with reasonable dimensional accuracy. The printability evaluation focused on the influence of volumetric flow rate and P/B ratio on layer uniformity, dimensional stability, and mechanical performance rather than on the direct effect of moisture content.

3D printing. Test samples were manufactured using an in-house modified Creality Ender3 S1 printer adapted for paste extrusion, as shown in **Figure 8**. A 4 mm nozzle was used for printing, and the layer height was set to 2 mm in Prusa Slicer software.

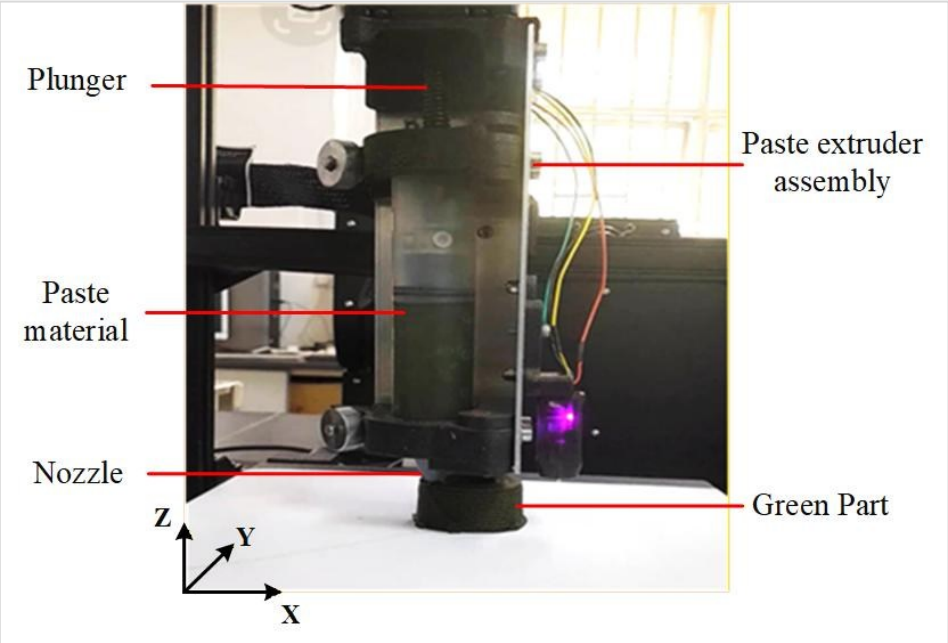


Figure 8. Paste extrusion 3D printing

For all test samples, the printing speed was fixed at 5 mm/s to identify the effect of volumetric flow rate. Volumetric flow rate was selected as a key factor because it directly governs the amount of material deposited per unit time, influencing filament continuity, internal void formation, dimensional accuracy, and mechanical behaviour [39]. Based on the preliminary parameter screening, three volumetric flow rate values were identified: 40 mm^3/s, 52 mm^3/s, and 64 mm^3/s, corresponding to extrusion multipliers of 100%, 130%, and 160%, respectively. Scenarios that resulted in nozzle clogging, discontinuous extrusion and excessive deformation were omitted. Two specimen geometries were designed for mechanical testing. For the compressive test, a hollow cylinder (outer diameter 40 mm, inner diameter 20 mm, and height 20 mm) was used to improve dimensional stability during printing and drying, as solid cylinders have been reported to exhibit deformation and cracking due to moisture gradients and shrinkage in paste-extruded materials [14], [40]. The hollow geometry enabled more uniform drying and reduced internal stresses, ensuring reliable and reproducible measurements. For flexural testing, rectangular bars (100 × 20 × 10 mm) were employed in a three-point bending test, consistent with ASTM D790 [41].

All printed test samples were dried at room temperature (~25.6 °C) under ambient laboratory conditions. No additional curing or thermal post-processing was applied. Each combination of biobased fraction, binder ratio, and flow rate was printed in triplicate, and results were averaged. The printing parameters for manufacturing samples, summarised in **Table 2,** were chosen to ensure reproducible mechanical performance [14].

Table 2. Printing parameters used for paste-extruding samples

Printing parameter	Considered value	Unit
Extruder speed	10	[mm/s]
Printing speed	5	[mm/s]
Nozzle diameter	4	[mm]
Specimens layer height	2	[mm]
Drying room temperature	~25.6	[°C]

Mechanical Characterisation of Paste-Extruded Parts

The printability and structural integrity of the paste-extruded samples were quantitatively evaluated through compressive and three-point bending flexural tests in JKUAT. For the compression test, the diameters and height of each hollow cylindrical specimen were measured using a digital calliper before testing. The compressive strength of specimens was analysed according to ASTM D695 using a SHIMADZU universal testing machine (UTM). The specimen was placed on the testing platform. The crosshead speed was adjusted to 5 mm/min, and the loading anvil was then moved downwards until it contacted the upper surface of the specimen. A compressive load was subsequently applied until failure. A force-displacement curve was recorded using TRAPESIUMX software. The compressive stress σ_C was calculated using eq. (3), where the load-bearing cross-sectional area was determined from the difference between the outer and inner circular areas of the hollow cylinder as:

$$\sigma_C = \frac{F_{max}}{\frac{\pi}{4}(D_0^2 - d_i^2)} \quad [MPa] \tag{3}$$

where F_{max} is the maximum compressive load [N], D_0 is outer diameter [mm], and d_i is the inner diameter [mm] of the specimen.

Similarly, flexural strength was measured in a three-point bending system per ASTM D790 using the same UTM. A digital calliper was used to measure all dimensions of the specimens before conducting the actual tests. Flexural loading was applied until failure, at which the loading nose was moved downwards at a constant crosshead speed of 5 mm/min to achieve contact of the nose with the specimen. The flexural strength σ_f was determined using eq. (4) for a rectangular bar cross-section:

$$\sigma_f = \frac{3F_{max}L}{2bh^2} \quad [MPa] \tag{4}$$

where F_{max} is the maximum bending force [N], L is the span length [mm], h is the specimen thickness [mm], and b is the specimen width [mm].

RESULTS AND DISCUSSION

This section briefly discusses the results of the experiments conducted in the study. It analyses the properties of the prepared powder materials, their effect on the printability in BJT and MEX techniques, and the mechanical performance of the manufactured samples.

Powder Characterisation

Biomass-based powder is highly susceptible to environmental conditions, which can affect moisture content, flow properties, and powder packing. To ensure uniformity and reproducibility, the powder samples were stored in moisture-controlled sealed containers at room temperature in the laboratory. The moisture content of each sample was measured before carrying out any tests or printing.

Physical and flow properties of powders. Standard tests were performed to determine the physical and flow properties of *P. juliflora* powders prepared from leaves, stems, and pods. Particle size fractions were obtained using a mechanical sieve (HAVER EML DIGITAL PLUS, **Figure 9a**) in accordance with ASTM C136/C136M-19 **[42]**, which provides standardised procedures for classifying fine and coarse aggregates.

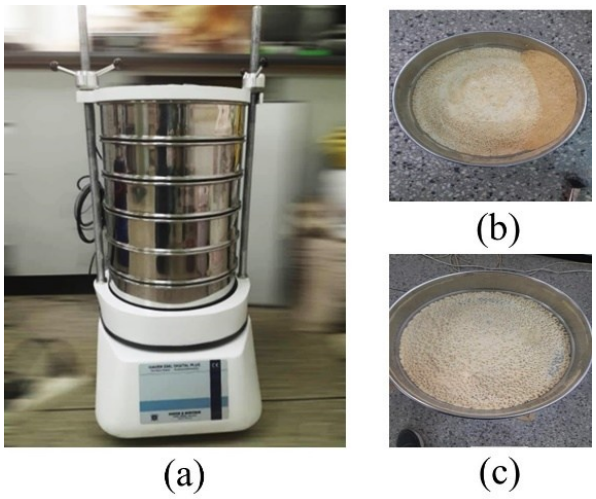


Figure 9. Mechanical sieving process: mechanical sieve shaker (a), fine and coarse pod powders after sieving (b), and adhered fine pod particles retained on larger mesh sizes (c)

Based on the powder availability at the mesh sizes, three particle-size fractions were selected: d < 355 µm for leaves and stems, and d < 500 µm for pods, to assess the effect of particle size on flowability. Leaves and stems demonstrated moderate hygroscopicity, with moisture contents of ~8% and 9%, respectively, as measured by a KERN DAB moisture analyser, and were stable under ambient conditions. Pod powders exhibited a lower moisture content of ~5% and were noted to be "sticky", indicating that the cohesion in powders may be attributable to surface chemistry rather than moisture content alone.

Bulk density (DIN ISO 60) and tap density (JEL STAV II) measurements indicated that leaves demonstrated consistent packing behaviour, while stems had slightly lower bulk and tapped density measurements. Pod powders showed higher bulk and tapped densities, although their stickiness made the bulk density measurement difficult without some effort to force the powder flow into the cylinder. This variation indicates how the flow characteristics of the biobased powders differ across their fractions. The results of the powder's physical characteristics are illustrated in **Figure 10** and summarised in **Table 3**.

As shown in Figure 10a, flowability depends on the material fraction and particle size. The flowability of leaf and stem powders increased with increasing particle size. For the fine fractions, *CI* values around 22.5% for leaves and 27.4% for stems were obtained, whereas for the coarse fractions, *CI* values were 10.2% and 23.7%, respectively. It implies that powders with larger particles are more flowable due to denser packing and less cohesion.

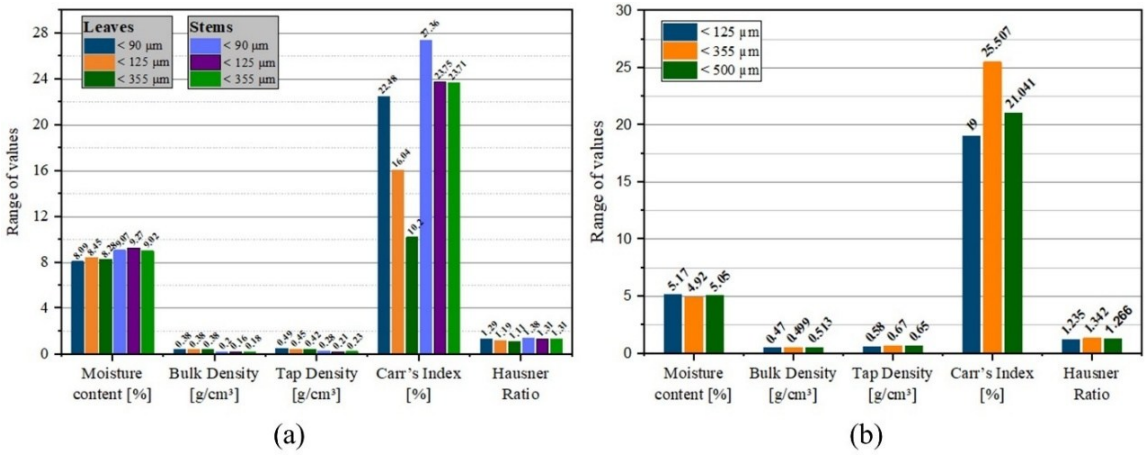


Figure 10. Physical and flow properties: leaf and stem powders (a), and pod powder (b)

Table 3. Physical and flow properties of Prosopis juliflora residue powders

Material	Sieve size [µm]	Parameter				
		Moisture content [%]	Bulk density [g/cm³]	Tap density [g/cm³]	Carr Index [%]	Hausner Ratio
Leaves	< 90	8.09	0.380	0.490	22.483	1.290
	90–125	8.45	0.378	0.450	16.037	1.191
	125–355	8.28	0.377	0.420	10.198	1.114
Stems	< 90	9.07	0.203	0.280	27.357	1.377
	90-125	9.27	0.160	0.210	23.746	1.311
	125-355	9.02	0.175	0.230	23.710	1.311
Pods	90-125	5.17	0.470	0.580	19.000	1.235
	125-355	4.92	0.499	0.670	25.507	1.342
	355-500	5.05	0.513	0.650	21.041	1.266

On the other hand, pod powders, as shown in **Figure 10b**, exhibit erratic profiles, with both fine and coarse fractions showing fair flowability with *CI* values of approximately 19% to 21%. The medium fraction, however, reaches ~25.5%, indicative of poor flow, possibly due to agglomeration resulting from particle shape. These results highlight the importance of particle morphology on flow performance, specifically for pod-based powders. Based on the standard powder classification for *CI* and *HR* in **Table 1**, the flowability revealed that leaf powders fall between "Excellent and Passable", stems between "Fair and Poor", and pods between "Fair and Poor". This variation indicates how the flow characteristics of the biobased powders differ across their fractions. These properties are important for binder jetting because they affect powder-bed formation, binder interaction, and overall printability.

Morphological analysis. SEM images at different magnifications show the powder characteristics of *P. juliflora* residues. As observed in **Figure 11a** and **Figure 11b**, angular and irregular particles with sharp edges and rough fractured surfaces. These particles can improve interlocking and packing, but they can also lead to increased friction during powder flow.

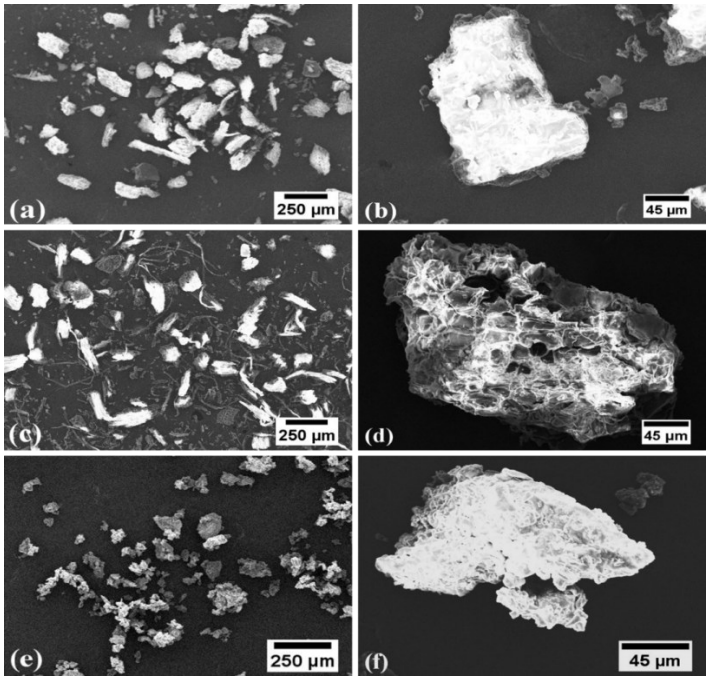


Figure 11. SEM images of Prosopis juliflora powder: leaves (a, b), stems (c, d), and pods (e, f)

Figure 11c and **Figure 11d** illustrate elongated, splintery fibrous particles with coarsely striated surfaces and porous interiors; these are characteristic of plant fibres. The finer granular particles (**Figure 11e** and **Figure 11f**) are smaller, more equiaxed, and less fibrous, but still irregular and porous. There is a greater tendency to agglomerate, which can negatively affect the powder's flowability and packing uniformity **[34]**. In general, the presence of angular, fibrous, and granular shapes in the biobased powder is indicative of the heterogeneity of the material, which will affect spreading, packing density, and reaction with the binder during a binder jetting process.

Particle size distribution analysis. PSD was analysed by laser diffraction to determine the particle size distributions of *P. juliflora* leaf, stem, and pod powders. The data summarised in **Table 4** give the characteristic particle diameters D_{10}, D_{50}, and D_{90} of *P. juliflora* residues, and powder data using volume-based cumulative distribution Q_3 and differential distribution q_3. D_{10} denotes the particle size below which 10% of the total powder volume lies and is a measure of the fine fraction of the powder. D_{50} is the median- size of the particles and D_{90} is the particle size below which 90% of the particle volume is contained, representing the coarse fraction. The Q_3 and q_3 volume-based PSD curves are illustrated in **Figure 12**. The Q_3 curves (indicating Cum values) show the cumulative contribution of particle sizes to the total powder volume, whereas the q_3 curves (Diff values) represent the frequency of particles at specific diameter ranges. Peaks in the q_3 curves indicate the most dominant particle size fractions.

Table 4. Particle size characteristics of Prosopis juliflora biobased residue powders

Cumulative diameter percentile [%]	Leaf powder [µm]	Stem powder [µm]	Pod powder [µm]
D_{10}	7.74	10.25	10.19
D_{50}	60.23	52.24	102.48
D_{90}	232.62	177.84	286.74

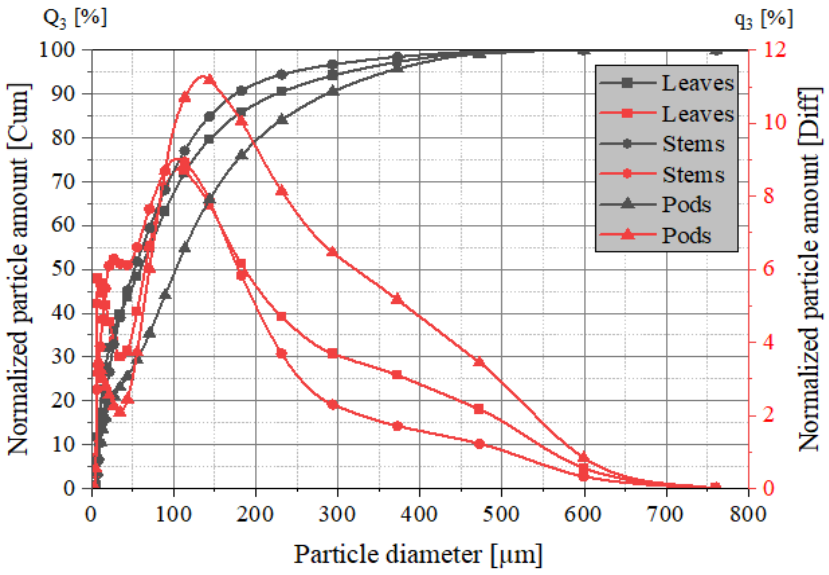


Figure 12. Volume-based Q3 and q3 PSD curves of Prosopis juliflora residue powders

The increased D_{50} and D_{90} values of the pod powder (D_{90} = 286.74 µm) point to the fact that coarser particles are present, and the lengthy tail (right-hand part) of the cumulative curve Q_3 for the pod powder also indicates this fact. This result can be explained by the pods' fibrous structure and mechanical hardness, which hinder effective milling. In contrast, powders of

leaves and stems showed finer particle distributions. The stem powder had the smallest median diameter and less dispersion, as realised by the lower values of D_{50} and D_{90}. Conversely, the median size and distribution of leaf powder were a little larger than that of stem powder, indicating that the powder was not uniformly broken through grinding. D_{90} value of leaf powder (232.62 µm) was higher, indicating the presence of coarse particles.

The results show that all powders exhibited dominant particle sizes within the range of 20–110 µm. This particle size range is considered suitable for BJT applications as it provides a good balance between powder flowability and packing density. For example, at particle diameters close to the median values (D_{50}), the Q_3 curves reach approximately 50%, confirming the representative average particle size for each powder. Beyond this range, Q_3 increases gradually, while q_3 decreases, indicating a reduced population of coarse particles. This behaviour confirms that most particles are concentrated in the fine-to-medium size range, with fewer large particles contributing to the distribution tail. The median size of particles (D_{50}) in pod powder was the highest at 102.48 µm, whereas the leaf and stem powders were 60.23 µm and 52.24 µm, respectively.

The difference PSD curves show a bimodal distribution across all powders, with a clear separation between fine and coarse particles. Bimodality is more pronounced in the leaf powder, which contains a high fraction of ultrafine particles ($d < 10$ µm) and coarse particles ($d > 200$ µm). This result could be caused by the heterogeneous microstructure of leaves, which consists of brittle tissues forming the fines and tougher veins that are not easily broken.

Considering all results, the observed differences in particle size properties indicate that plant morphology affects powder processing behaviour. These differences highlight the importance of controlling particle size and material type when producing *P. juliflora* powders for additive manufacturing via 3D printing.

Powder-Bed Formation Assessment of Residue Materials in Binder Jetting

The leaf- and stem-derived powders exhibited good spreading behaviour in the "ZPrinter 310" 3D printer, enabling the formation of a smooth and continuous powder bed with uniform layer thickness and consistency, as shown in **Figure 13a** and **Figure 13b**. Consequently, these powders enabled us to successfully produce cube-shaped green parts with a stable geometry (**Figure 14a** and **Figure 14b**).

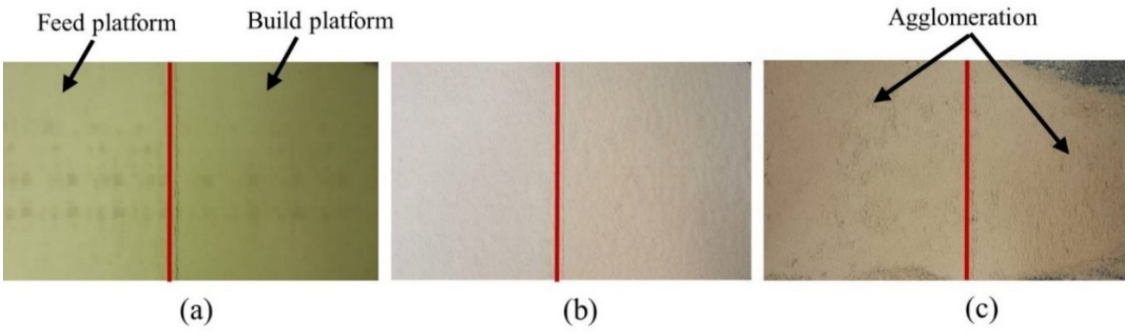


Figure 13. Powder spreadability evaluation images for: leaf (a), stem (b), and pod (c) powders

The powders originating from the pods, on the other hand, showed poor powder-bed formation and inconsistent layer deposition. Their stickiness led to problematic handling: during sieving, some particles would stick to the sieve mesh, and finer particles would build up within the coarser sieve fractions, as illustrated in the subsection on powder properties (**Figure 9b** and **Figure 9c)**. The same problem occurred during spreading, as significant agglomeration also caused clumping and uneven spreading, thereby preventing the formation of continuous layers (**Figure 13c**).

This behaviour not only hindered the formation of a uniform powder bed and caused uneven layer deposition but also resulted in caking beyond the intended CAD design boundaries, making it difficult to de-powder the intended shape from the unused powder, as illustrated in **Figure 14c**. The stickiness of the powders was a greater concern than particle size in limiting the use of pod-based powders. The specimens, primarily produced from leaves and stems, were evaluated for powder-bed formation, green-part integrity, and overall printing performance. No standardised mechanical testing was conducted at this stage of the research.

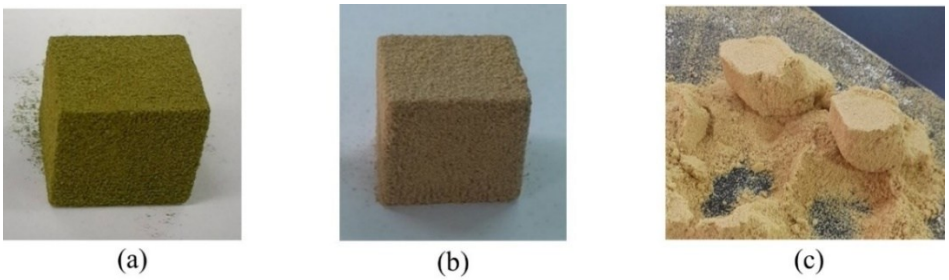


Figure 14. Printed green parts produced from: leaf (a), stem (b), and pod (c) powders

Justification of *Prosopis Juliflora* Residues for Binder Jetting Evaluation

The residue materials of *P. juliflora* were assessed for BJT owing to their physical, flow, morphological properties, PSD, and powder-bed formation behaviour. This subsection breaks down the observations by inherent material characteristics to give an overall explanation of the relative performance of the biobased residue materials. Leaf residues were found to be the most appropriate material. They had uniform sieving, good bulk and tapped densities, favourable flow indices, and angular-to-irregular particle shapes, which led to successful layer formation and stable green parts. These characteristics could explain the formation of successful powder beds, the provision of uniform layers, and the maintenance of stable green parts, highlighting the leaf residues being the most critical determinant of BJT feasibility. The hard and fibrous nature of the stem residue powders, despite requiring labour-intensive preprocessing such as reducing to small chips, was identified as slightly lower in flowability, allowing them to form continuous layers with acceptable printability. In contrast, pod residues were the least suitable. Although they exhibited higher bulk and tapped densities, the powders showed strong agglomeration and stickiness, which hindered uniform spreading and powder-bed formation.

To quantify the overall suitability of the residue powders for BJT, a numerical scale from 1 to 5 was used, with 1 representing inferior performance and 5 indicating excellent performance. **Table 5** summarises assigned ratings, indicating the material properties and their influence on the formation and integrity of powder beds.

Table 5. Suitability of Prosopis juliflora residue powders for binder jetting, based on powder characteristics and powder-bed formation (rating: 1 = poor, 5 = excellent)

Property/Characteristics	Suitability rating of *P. juliflora* residue material		
	Leaves	Stems	Pods
Moisture content	4	4	5
Bulk and tapped density	4	3	4
Flow indices	4	3	3
Morphology	3	3	4
PSD	5	5	4
Powder-bed formation and layer consistency	5	5	2
Tendency to agglomerate	5	5	1
Overall suitability	5	4	2

While the present study focused on processing powders in their natural state to establish baseline feasibility, the strong stickiness and agglomeration of pod-derived powders, due to surface sugars, oils, and extractives, remain major limitations for processability. This behaviour indicates that the use of alternative preprocessing techniques, such as separating seeds from pods, solvent extraction, or mild alkali treatment, might help overcome cohesion to improve powder flow, allowing for the incorporation of pod residues in BJT.

Evaluation of Printability Using Paste Extrusion

The *P. julifora* residues exhibited a sticky nature when mixed with water, adversely affecting their handling and printability. The high level of stickiness hindered continuous strand extrusion and the dimensional stability of parts on the print bed. To overcome this problem, the *P. juliflora* powders were mixed with two different binder formulations. The higher the binder content in the powder blend, the lower the paste stickiness, as these bound particles form a more cohesive paste and provide greater internal bonding, resulting in more stable, extrudable pastes.

Another factor that was very important for paste flow behaviour was particle size. The particle size range was thus chosen to be $d < 125$ µm, which facilitated easier extrusion through the nozzle and reduced the risk of clogging. This size range also helped increase the paste's homogeneity. The bed heating was not applied during printing to prevent early drying and ensure a steady flow of paste during extrusion.

Moisture content and paste formulation characteristics. In all materials, there was a systematic increase in moisture content, accompanied by a corresponding increase in binder content from 15 wt.% to 30 wt.%. The increased moisture content in 30 wt.% CMC can be explained by CMC's hydrophilic character, which absorbs water and forms a viscous polymer network at high levels, thereby increasing the paste yield stress and resistance to flow [43]. Figure 15 shows the homogeneous, extrudable paste samples for each biobased fraction, and Table 6 summarises the moisture contents required to achieve the required paste properties.



(a) (b) (c)

Figure 15. Results of paste preparation from the powders of leaf (a), stem (b), and pod (c)

The highest moisture content, 68% by total weight, was observed in stem-based pastes. These pastes showed resistance to extrusion at the lowest moisture levels. In contrast, the moisture content was lower in pod-based pastes. The moisture content of 54 wt.% was the lowest at 15 wt.% CMC, and the paste showed improved flowability. These differences in moisture content, which depend on the P/B ratio formulation, directly affected extrusion stability and drying behaviour.

Table 6. Prosopis juliflora paste formulations as used for paste extrusion 3D printing

Material	Binder ratio [wt.%]	Moisture content [wt.%]
Leaf	15	56
	30	63
Stem	15	63
	30	68
Pod	15	54
	30	64

Effect of volumetric flow rate on extrusion stability and layer formation. The printability of the different biobased residues was investigated by varying the paste volumetric flow rate from 40 mm^3/s to 64 mm^3/s. The impact of volumetric flow rate on print quality is demonstrated using cylindrical and rectangular bar specimens. **Figure 16** shows typical green-state prints of a pod-based paste containing 15 wt.% CMC. Both specimen shapes could be printed at the baseline flow rate of 40 mm^3/s (**Figure 16a** and **Figure 16b**); however, the extrusion was not completely stable. The paste flow was nonuniform, and local drying at the nozzle caused broken filaments, uneven layer deposition, and incomplete filling of the structured geometry. These characteristics indicate under-extrusion, due to insufficient material deposition relative to the paste viscosity.

Extrusion stability and layer formation improved dramatically when the flow rate was increased to 52 mm^3/s (**Figure 16c** and **Figure 16d**). The filaments were deposited continuously, the layers were laid evenly, and the parts being printed were printed well. The rate of material flow ensured a balance between material flow and nozzle motion, thereby forming clear cylindrical walls and better rectangular edges. This state provided an enhanced green-state structural integrity.

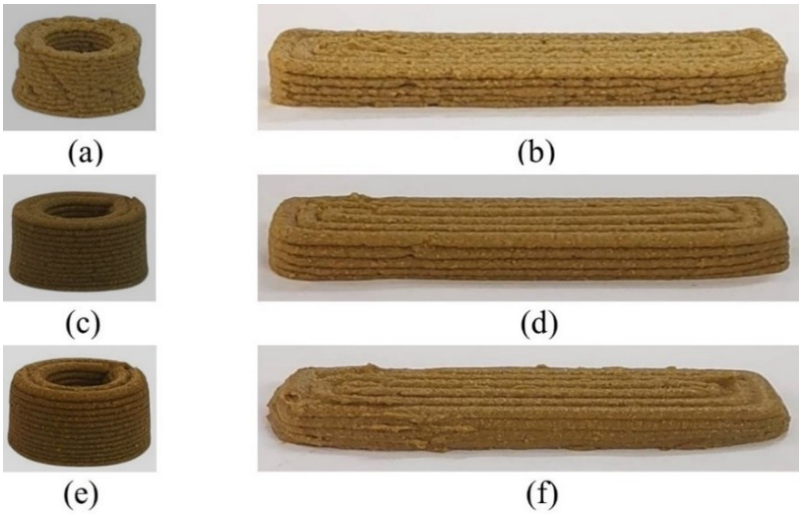


Figure 16. Green parts of pod-based paste at 15 wt.% CMC for cylindrical and rectangular bar specimens printed at flow rates of 40 mm3/s (a, b), 52 mm3/s (c, d), and 64 mm3/s (e, f)

Increasing the flow rate to 64 mm^3/s (**Figure 16e** and **Figure 16f**) allowed the extrusion process to continue, but the high material deposition led to over-extrusion. This development resulted in filament compression, wall thickening, and overfilling of print features. The rectangular bar specimens, especially, had rounded sides and lost sharp angles, whereas the cylindrical specimens were printable but showed evidence of excess material deposition.

In general, the described findings indicate that in biobased MEX, a high volumetric flow rate affects the extrusion stability and the layer formation. Though specimens were

satisfactorily printed over the entire range of flow rates, 52 mm^3/s provided the best balance of dimensional stability.

Drying behaviour and dimensional stability of samples. During *P. juliflora* printing, both the material fraction and P/B ratio had strong effects. Although minor environmental variability occurred, the consistent room conditions allowed sufficient drying, maintaining dimensional stability and reproducible mechanical performance. **Figure 17a–Figure 17d** show the typical dried samples of leaf and stem residues printed with 15 wt.% CMC and 52 mm^3/s flow rate. Stable drying behaviour was observed in both leaf- and stem-based specimens in both P/B ratio formulations. Despite moderate shrinkage of the 30 wt.% CMC, the printed samples remained structurally stable and dimensionally quantifiable. These studied residues had fibrous and particulate morphologies, which probably decreased drying-induced stresses on the capillaries and thus prevented undue deformation. No collapse was observed, indicating that the leaf and stem fractions are not as sensitive to binder content during drying.

In contrast, the pod-based specimens were highly dependent on the binder ratio. **Figure 18a** demonstrates that specimens printed at 15 wt.% CMC maintained their geometric integrity and showed little shrinkage during drying, including cone formation in the case of cylindrical geometry, yet remained functional. Nevertheless, samples printed at 30 wt.% CMC (**Figure 18b**) showed pronounced deformation during drying. In this case, the samples are characterised by inward wall collapse, edge rounding, and partial closure of internal features, leading to dimensional instability and loss of functional geometry. The greater the binder content, the more moisture was retained, and capillary forces induced inward wall deformation, causing internal features to collapse and resulting in a loss of dimensional stability.

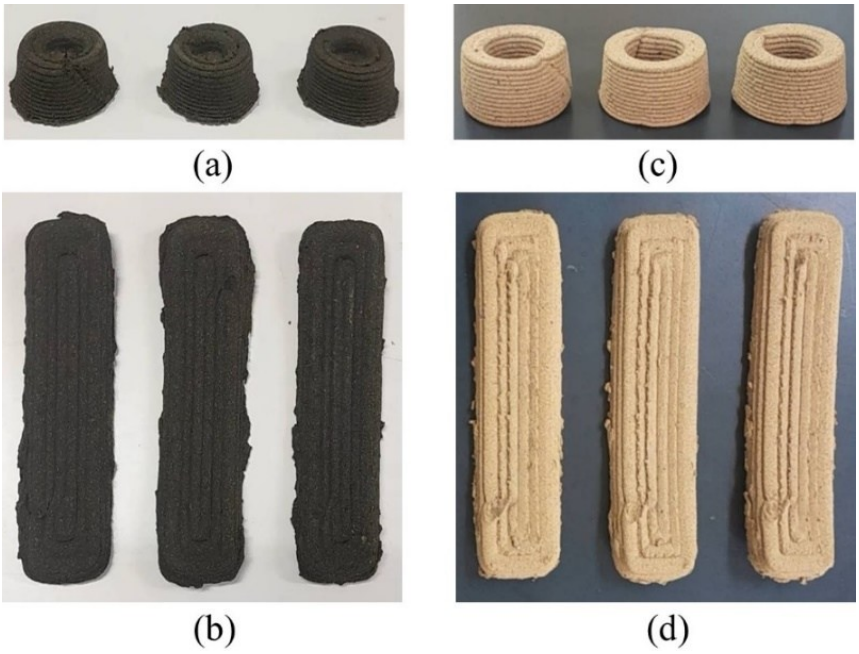


Figure 17. Dried printed samples at 15 wt.% CMC and 52 mm3/s of flow rate for cylindrical and rectangular bars: leaf (a, b) and stem (c, d) residues

These findings reveal the important role of the binder content on drying stability and show that 15 wt.% CMC is better suited to pod-based materials. Overall, the minor environmental variations had little impact due to consistent laboratory conditions. The main factors that made a difference were the material's morphology and the binder proportion, demonstrating the importance of binder content for stable drying.

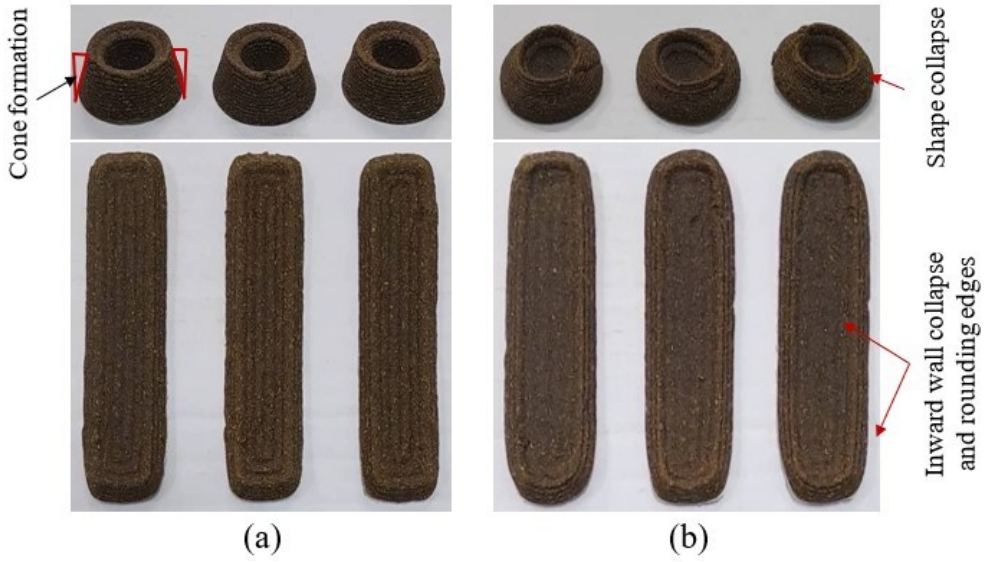


Figure 18. Dried pod specimens at 52 mm3/s flow rate: 15 wt.% CMC (a), and 30 wt.% CMC (b)

Mechanical Testing of Paste-Extruded Samples

This subsection briefly presents the mechanical property measurements of printed specimens obtained from the different material fractions.

Compressive test. The compressive behaviour of the printed specimens was influenced by the material fractions (leaf, stem, and pod), P/B ratio, and flow rates. The findings of the two formulations are provided in **Figure 19a** and **Figure 19b**. In leaf-based samples at 15 wt.% CMC, compressive strength decreased linearly with volumetric flow rate, with values of ~1.99 MPa at 40 mm^3/s flow rate and ~1.02 MPa at 64 mm^3/s flow rate. This observation indicated that poor layer definition and increased internal defects occurred as flow rates increased, thereby lowering load-bearing capacity. On the other hand, samples containing 30 wt.% CMC showed a definite increase in compressive strength to 6.28 MPa at a 52 mm^3/s flow rate and a slight decrease to 5.8 MPa at a 64 mm^3/s flow rate. This tendency implies that high binder content promotes particle bonding and interlayer cohesion until the optimal deposition level, after which over-deposition adversely affects structural integrity.

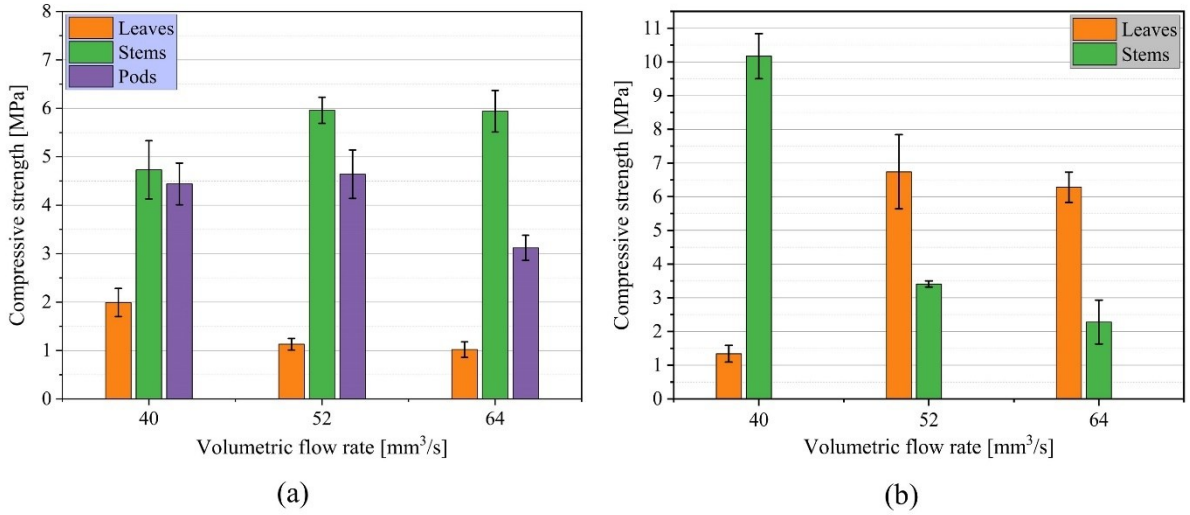


Figure 19. Compressive strength of printed samples: 15 wt.% CMC (a) and 30 wt.% CMC (b)

The compressive strength of the stem-based samples was the highest of all material fractions. At 15 wt.% CMC, the compressive strength was highest at 52 mm^3/s (nearly 6 MPa), slightly reduced at 64 mm^3/s, and lowest at 40 mm^3/s (approximately 4.73 MPa). This trend shows enhanced densification and inter-layer bonding at a middle flow rate, at which pore formation begins due to over-deposition of the material. Nevertheless, at a higher binder content of 30 wt.% CMC, a significant reduction in compressive strength was noted as the volumetric flow rate increased. As indicated in **Figure 19b**, compressive strength dropped with increased flow rate from ~10.17 MPa to 2.28 MPa. This loss is due to over-binding and moisture retention, both of which weaken the dried structure and make it easier for internal voids to form.

For pod-based specimens, compressive strength could be measured only at a CMC content of 15 wt.%, as previously explained in the subsection on drying behaviour. The volumetric flow rate influenced the compressive test, with a maximum at 52 mm^3/s and a slightly lower value at 64 mm^3/s. This action signifies increased consolidation and particle rearrangement, up to a certain flow rate, beyond which excessive material deposition negatively influences structural stability. At 30 wt.% CMC, the samples did not maintain dimensional stability during drying, and no quantifiable compressive strength was achieved.

Based on the results, compressive strength is highly influenced by both the binder ratio and the volumetric flow rate, and their influence are closely related to each other. Varying the binder ratio to 30 wt.% CMC significantly increased strength and, in several cases, resulted in higher compressive strength. However, this improvement did not occur for all materials and flow rates in the same way. Rather, the impact of binder content depended on the amount of material deposited and the plant fraction used. These findings indicate that the binder ratio cannot be assessed independently, as its influence on strength is also affected by volumetric flow rate and material.

Flexural test. **Figure 20a** and **Figure 20b** show that the flexural strength results for leaf, stem, and pod samples followed a pattern similar to the compressive tests, but highlighted different strengths. At 15 wt.% CMC, the best flexural strength was observed in pod-based samples with the highest flexural strength of ~5.69 MPa at 40 mm^3/s flow rate, whereas upon increasing to 52 mm^3/s and 64 mm^3/s, the flexural strength of the specimens declined to ~4.17 MPa and 3.33 MPa, respectively. This decrease suggests that the increased flow rate can cause particle misalignment or internal voids, thereby reducing the material's capacity to withstand bending.

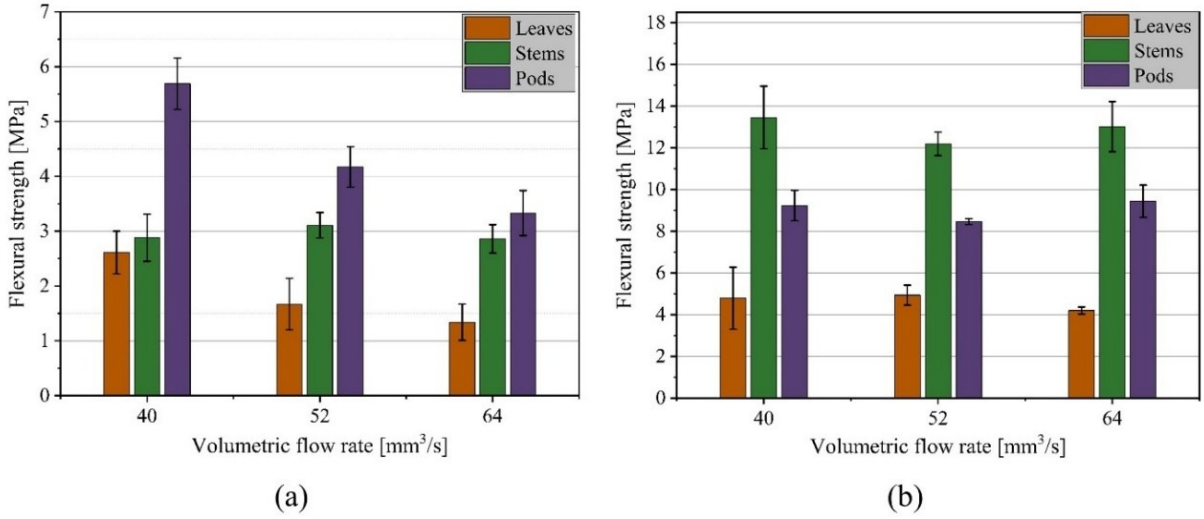


Figure 20. Flexural strength of printed samples: 15 wt.% CMC (a) and 30 wt.% CMC (b)

Stem-based samples exhibited moderate flexural strength (~2.86 MPa to 3.11 MPa) with a small rise at the 52 mm^3/s flow rate and a small drop at the 64 mm^3/s flow rate. This trend indicates enhanced layer deposition at moderate flow rates and the development of structural defects at higher flow rates. In leaf-based samples, the least flexural strength (~1.34 MPa to 2.61 MPa) was recorded, showing a minimal contribution to mechanical resistance in bending. There was a significant increase in overall flexural strengths at 30 wt.% CMC, and with stems, pods, and leaves recording the highest flexural strengths of 13.45 MPa, 9.44 MPa, and 4.94 MPa, respectively. Increased binder content enhanced particle cohesion and matrix-particle interactions, stabilising performance across volumetric flow rates and limiting sensitivity to flow-induced defects. Remarkably, the relative contribution of powder type varied with binder content: pods gave better results at low CMC, while stems gave better flexural results at high CMC, which explains the importance of the matrix density in load transfer and structural integrity.

The findings show that the flexural strength is influenced by both the binder ratio and the volumetric flow rate, and that material fraction effects are present. The lower binder ratio is more dependent on flow rate, and the higher binder ratio is more likely to enhance flexural strength and diminish the effect of deposition rate. These results reveal that bending behaviour results from the combined effects of material composition, binder percentage, and processing parameters, rather than from a single factor.

CONCLUSIONS

This study investigated the process feasibility and mechanical performance of *P. juliflora* biobased residue materials as alternative feedstocks for AM through BJT and MEX processes. From the analysis of experimental results, it can be concluded that:

- Material properties: leaf and stem powders exhibited better physical characteristics, including packing, flowability, and PSD. On the other hand, pod powders showed greater cohesion and a tendency to agglomerate, resulting in poor powder-bed formation and inconsistent drying behaviour of paste-extruded parts.
- Powder-bed formation (BJT): leaf and stem powders showed good spreadability and formed stable powder beds, resulting in stable green parts. However, pod powders did not spread uniformly and could not be printed successfully under the tested conditions. These results suggest that process-level printability in BJT depends primarily on the powder morphology and flow properties.
- Paste-extrudability (MEX): regarding the MEX process, all fractions achieved stable extrusion and shape retention at the optimal volumetric flow rate of 52 mm^3/s. Higher binder content improved dimensional stability and overall mechanical performance, although pod-based materials performed poorly in compressive tests.
- Mechanical performance: paste-extruded components underwent quantifiable mechanical testing. The peak compressive strength of 10.17 MPa was achieved in stem-based specimens, representing a 50.9% increase over leaf-based specimens and a 119.2% increase over pod-based specimens. Likewise, the highest flexural strength was 13.45 MPa in the stem-based samples, corresponding to a 172.3% increase over the leaf-based samples and 42.5% increment to the pod-based samples. Increased binder content enhanced inter-particle bonding and mechanical properties across all fractions.
- Sustainability and economic relevance: this work shows how the invasive species *P. juliflora* can be valorised into usable AM materials via a simple, environmentally benign processing pathway, managing invasive species and promoting the principles of the circular economy.
- Featured application: the developed biobased materials can be used in low-load-bearing components, packaging, and prototyping applications where moderate mechanical performance, low density, and low production cost are required.

In summary, this study is the first to demonstrate that *P. juliflora* residue materials can be utilised as a viable, low-cost, and eco-friendly raw material for AM technologies. Leaf powder is the most suitable filler material for BJT due to its excellent flowability and uniform layer formation, followed by stem powder. In contrast, stem-based materials showed outstanding performance in MEX owing to their fibrous structure. All fractions yielded printable components with satisfactory mechanical properties in MEX. However, the mechanical properties of paste extrusion-printed parts depend primarily on the material used, the amount of binder, and the printing conditions.

The findings provide a solid foundation for ongoing research on detailed mechanical testing and the optimisation of binder-jetted parts, including post-processing, surface treatment techniques, and the long-term durability and biodegradability of materials. These research directions will further support the potential of *P. juliflora* plant residues as a sustainable biobased material for processing into AM and promote the development of environmentally responsible manufacturing solutions.

ACKNOWLEDGMENTS

The authors would like to acknowledge the financial support of the African Union (AU) through the Pan African University Institute for Basic Sciences, Technology and Innovation (PAUSTI); the Mechanical and Mechatronic Engineering Department at Jomo Kenyatta University of Agriculture and Technology (JKUAT), Kenya, for technical and laboratory assistance; and Raya University, Ethiopia, for sponsoring the study to attend abroad.

NOMENCLATURE

Symbols

b	Width of specimen	[mm]
D_o	Outer diameter	[mm]
d_i	Inner diameter	[mm]
F	Force/load applied	[N]
h	Thickness of specimen	[mm]
L	Length of specimen	[mm]
m	Mass	[kg]
Q_3	Cumulative distribution	[%]
q_3	Differential distribution	[%]
V	Volume	[cm^3]

Greek letters

ρ_{bulk}	Bulk density	[g/cm^3]
ρ_{tap}	Tap density	[g/cm^3]
σ_c	Compressive stress	[MPa]
σ_f	Flexural strength	[MPa]

Abbreviations

3D	Three Dimensional
AI	Artificial Intelligence
AM	Additive Manufacturing
ASTM	American Society for Testing and Materials
BJT	Binder Jetting Technology
CAD	Computer-Aided Design
CI	Carr Index
CMC	Carboxymethyl Cellulose

FFF	Fused Filament Fabrication
HR	Hausner Ratio
HSS	High-Speed Sintering
MEX	Paste Extrusion (Material Extrusion)
PSD	Particle Size Distribution
rHDPE	Recycled High Density Polyethylene
SED	Secondary Electron Detector
SEM	Scanning Electron Microscope
SLS	Selective Laser Sintering
UTM	Universal Testing Machine

REFERENCES

1. Srivastava, M., Rathee, S., Patel, V., Kumar, A. and Koppad, P. G., A review of various materials for additive manufacturing: Recent trends and processing issues, *J. Mater. Res. Technol.*, Vol. 21, pp 2612-2641, 2022, https://doi.org/10.1016/j.jmrt.2022.10.015.
2. Saleh Alghamdi, S., John, S., Roy Choudhury, N. and Dutta, N. K., Additive Manufacturing of Polymer Materials: Progress, Promise and Challenges, *Polymers (Basel)*, Vol. 13, 753, 2021, https://doi.org/10.3390/polym13050753.
3. Tebianian, M., Aghaie, S., Razavi Jafari, N., Elmi Hosseini, S., Pereira, A., Fernandes, F., Farbakhti, M., Chen, C. and Huo, Y., A Review of the Metal Additive Manufacturing Processes, *Materials (Basel)*, Vol. 16, 7514, 2023, https://doi.org/10.3390/ma16247514.
4. Kamran, M., Saxena A., Comprehensive Study on 3D Printing Technology, *MIT International Journal of Mechanical Engineering*, Vol. 6, No. 2, pp 63-69, 2016, https://www.researchgate.net/publication/310961474_A_Comprehensive_Study_on_3D_Printing_Technology, [Accessed: May. 26, 2026].
5. Reddy, N. S., Koti, H., Sajid, P. M., Velu, C. M., Velagaleti, S. K., Prasanna, P. L., Balasaranya, K. and Rajeswaran, N., Sustainable AI-Driven Hybrid Manufacturing Using Additive and Subtractive Processes, *Eng. Technol. Appl. Sci. Res.*, Vol. 15, pp 28878-28884, 2025, https://doi.org/10.48084/etasr.11785.
6. Alghamdi, A., Enhancing 3D Printing Workflows through Multi-Objective Optimization and Reinforcement Learning Techniques, *Eng. Technol. Appl. Sci. Res.*, Vol. 15, pp 21300-21305, 2025, https://doi.org/10.48084/etasr.10101.
7. Sekula, R., Leis, A., Wassong, A., Preuss, A., Hanning, H., Kemnitzer, J., Wimmer, M., Kuniewski, M. and Mikrut, P., Additive Manufacturing of Biobased Material Used in Electrical Insulation: Comparative Studies on Various Printing Technologies, *Polymers (Basel)*, Vol. 17, 2248, 2025, https://doi.org/10.3390/polym17162248.
8. Su, J., Ng, W. L., An, J., Yeong, W. Y., Chua, C. K. and Sing, S. L., Achieving sustainability by additive manufacturing: a state-of-the-art review and perspectives, *Virtual Phys. Prototyp.*, Vol. 19, e2438899, 2024, https://doi.org/10.1080/17452759.2024.2438899.
9. Jiang, H., Yang, X. and Wang, H., Preparation and characterization of starch-based binders for binder jetting, *RSC Adv.*, Vol. 14, pp 32506-32516, 2024, https://doi.org/10.1039/D4RA05411C.
10. Mohd Yusoff, N. H., Chong, C. H., Wan, Y. K., Cheah, K. H. and Wong, V.-L., Optimization strategies and emerging application of functionalized 3D-printed materials in water treatment: A review, *J. Water Process Eng.*, Vol. 51, 103410, 2023, https://doi.org/10.1016/j.jwpe.2022.103410.
11. Ma, Y., Potappel, J., Schutyser, M. A. I., Boom, R. M. and Zhang, L., Quantitative analysis of 3D food printing layer extrusion accuracy: Contextualizing automated image analysis with human evaluations, *Curr. Res. Food Sci.*, Vol. 6, 100511, 2023, https://doi.org/10.1016/j.crfs.2023.100511.

12. Micke, L., Kühnel, L., Mwangi, W., Karanja, K. and Zeidler, H., Conversion of bio-based residues into AM materials as a sustainable and cost-effective approach: example of water hyacinths in Kenya, Proceedings of the 2023 Rapid.Tech Fachkongress Conference, Erfurt Messe, Germany, pp 60-67, 2023, https://api.pageplace.de/preview/DT0400.9783446479425_A46969160/preview-9783446479425_A46969160.pdf, [Accessed: May. 26, 2026].
13. Khan, F., Shakil Arman, M., Sanders, J., Meraj Pasha, M., Mazedur Rahman, A., Pei, Z. and Dong, T., Binder Jetting 3D Printing Utilizing Waste Algae Powder: A Feasibility Study, *Intell. Sustain. Manuf.*, Vol. 1, 10016, 2024, https://doi.org/10.70322/ism.2024.10016.
14. Hussein, M. H., Mutava, L. M., Waititu, D. W., Kimotho, J. K., Mwangi, W., Micke, L., Ronoh, E. K. and Karanja, S. K., Investigation of Mechanical Properties of Printed Rice Husk Parts Using an Inhouse Modified Paste Extrusion Printer, Proceedings of the 2023 Sustainable Research and Innovation Conference, Kenya, pp 1-5, 2023, https://www.researchgate.net/publication/384232290_Investigation_of_Mechanical_Properties_of_Printed_Rice_Husk_Parts_Using_an_Inhouse_Modified_Paste_Extrusion_Printer, [Accessed: May. 26, 2026].
15. Andanje, M. N., Mwangi, J. W., Mose, B. R. and Carrara, S., Development of additive manufacturing biofilaments from recycled high-density polyethylene and rice husks: optimization of extrusion parameters, *J. Agric. Sci. Technol.*, Vol. 23, pp 90-102, 2024, https://doi.org/10.4314/jagst.v23i4.6.
16. Bah, M. B., Mwangi, J. W. and Kabini, K., Fused Filament Fabrication of Recycled HDPE and Cactus Composite as a Biobased Material, *Eng. Reports*, Vol. 7, e70121, 2025, https://doi.org/10.1002/eng2.70121.
17. Santhosh, M. S., Karthikeyan, G., Sasikumar, R., Hariharan, R. and Mohanraj, R., Mechanical and morphological behaviour of rice husk/prosopis juliflora reinforced bio composites, *Mater. Today Proc.*, Vol. 27, pp 556-560, 2020, https://doi.org/10.1016/j.matpr.2019.12.021.
18. Subbiah, D., Mani, N., Selvaraju, S. and Thangavelu, E., Characterization and Analysis of Mechanical and Morphological Properties of Hybrid Composite Material from Prosopis Juliflora and Phoenix Sylvestris for Engineering Applications, *Materials Science (Medžiagotyra)*, Vol. 30, No. 4, 2024, https://doi.org/10.5755/j02.ms.37897.
19. Debella, H. A., Ancha, V. R. and Atnaw, S. M., Production, optimization, and characterization of Ethiopian variant Prosopis juliflora based biodiesel, *Heliyon*, Vol. 9, e15721, 2023, https://doi.org/10.1016/j.heliyon.2023.e15721.
20. Rao, T. S. S. B., Gnanaprakasam, M., Manimaran, R., Balasubramanian, D., Kale, U. and Kilikevičius, A., Sustainable synthesis and advanced optimization of Prosopis juliflora biomass catalyst for efficient biodiesel production and environmental impact assessment, *Sci. Rep.*, Vol. 15, 4472, 2025, https://doi.org/10.1038/s41598-025-88355-z.
21. Fang, X., Zu, Y., Ma, Q. and Hu, J., State of the art of metal powder bonded binder jetting printing technology, *Discov. Mater.*, Vol. 3, 2023, https://doi.org/10.1007/s43939-023-00050-w.
22. Hussain, M. I., Shackleton, R., El-Keblawy, A., González, L. and Trigo, M. M., Impact of the Invasive Prosopis juliflora on Terrestrial Ecosystems, in: *Prosopis juliflora in Africa*, Springer Nature Switzerland AG, pp 223-278, 2021, https://doi.org/10.1007/978-3-030-73245-5_7.
23. Al-Assaf, A., Tadros, M. J., Al-Shishany, S., Stewart, S., Majdalawi, M., Tabieh, M. and Othman, Y. A., Economic Assessment and Community Management of Prosopis juliflora Invasion in Sweimeh Village, Jordan, *Sustainability*, Vol. 12, 8327, 2020, https://doi.org/10.3390/su12208327.

24. Mungoche, J., Wasonga, O. V., Ikiror, D., Akala, H., Gachuiri, C. and Gitau, G., Prosopis juliflora (Sw.) DC in the drylands: A review of invasion, impacts and management in Eastern Africa, *Sustain. Environ.*, Vol. 11, 2025, https://doi.org/10.1080/27658511.2025.2521946.
25. Pasha, S. V. and Reddy, C. S., Global spatial distribution of Prosopis juliflora - one of the world's worst 100 invasive alien species under changing climate using multiple machine learning models, *Environ. Monit. Assess.*, Vol. 196, 2024, https://doi.org/10.1007/s10661-024-12347-1.
26. Kishoin, V., Tumwesigye, W., Turyasingura, B., Wilber, W., Chavula, P., Gweyi-Onyango, J. P., Kader, S., Spalevic, V., Skataric, G. and Jaufer, L., The negative and positive impacts of Prosopis juliflora on the Kenyan and Ethiopian ecosystems: A review study, *Not. Sci. Biol.*, Vol. 16, pp 1-15, 2024, https://doi.org/10.15835/nsb16111832.
27. Gu, B.-J., Wang, J., Wolcott, M. P. and Ganjyal, G. M., Increased sugar yield from pre-milled Douglas-fir forest residuals with lower energy consumption by using planetary ball milling, *Bioresour. Technol.*, Vol. 251, pp 93-98, 2018, https://doi.org/10.1016/j.biortech.2017.11.103.
28. KERN & SOHN GmbH, Operating Manual – Moisture Analyzer DAB 100-3, Version 1.3, 2018, https://manualzz.com/doc/81329855/kern-dab-moisture-analyser-operating-manual, [Accessed: Jul. 8, 2025].
29. ASTM International, Test Methods for Apparent Density, Bulk Factor, and Pourability of Plastic Materials, ASTM D1895-17, 2017, https://doi.org/10.1520/D1895-17.
30. ISO 60:2023, Plastics - Determination of apparent density of material that can be poured from a specified funnel, Geneva, Switzerland, 2023, https://standards.iteh.ai/catalog/standards/cen/cd643f0f-d001-4f71-8be8-6e51f78a394e/en-iso-60-2023, [Accessed: Jul. 9, 2025].
31. ISO 3953:2025, Metallic powders - Determination of tap density, International Organization for Standardization, Geneva, Switzerland, 2025, https://www.iso.org/obp/ui/en/#iso:std:iso:3953:ed-5:v1:en, [Accessed: Jul. 9, 2025].
32. United States Pharmacopeial Convention, USP <1174> Powder Flow, 2024, https://www.usp.org/harmonization-standards/pdg/general-chapters/powder-flow, [Accessed: Jul. 20, 2025].
33. PharmaSciences, Compressibility Index and Hausner Ratio, 2022, https://pharmasciences.in/compressibility-index-and-hausner-ratio/, [Accessed: Jul. 20, 2025].
34. Islam, S. F., Hawkins, S. M., Meyer, J. L. L. and Sharman, A. R. C., Evaluation of different particle size distribution and morphology characterization techniques, *Addit. Manuf. Lett.*, Vol. 3, 100077, 2022, https://doi.org/10.1016/j.addlet.2022.100077.
35. Clares, A. P. and Manogharan, G., Discrete-Element Simulation of Powder Spreading Process in Binder Jetting, and the Effects of Powder Size, Proceedings of the ASME Manufacturing Science and Engineering Conference, Vol. 1, p. V001T01A009, 2021, https://doi.org/10.1115/MSEC2021-63351.
36. Lv, X., Ye, F., Cheng, L., Fan, S. and Liu, Y., Binder jetting of ceramics: Powders, binders, printing parameters, equipment, and post-treatment, *Ceram. Int.*, Vol. 45, pp 12609-12624, 2019, https://doi.org/10.1016/j.ceramint.2019.04.012.
37. Huang, J. and Li, L., 3D printing of cellulose-based biomaterials: A review, *BME Horiz.*, Vol. 3, 138, 2025, https://doi.org/10.70401/bmeh.2025.0001.
38. Albelo, I., Raineri, R. and Salmon, S., Materials and Methods for All-Cellulose 3D Printing in Sustainable Additive Manufacturing, *Sustain. Chem.*, Vol. 5, pp 98-115, 2024, https://doi.org/10.3390/suschem5020008.

39. Lendvai, L., Fekete, I., Rigotti, D. and Pegoretti, A., Experimental study on the effect of filament-extrusion rate on the structural, mechanical and thermal properties of material extrusion 3D-printed polylactic acid (PLA) products, *Prog. Addit. Manuf.*, Vol. 10, pp 619-629, 2025, https://doi.org/10.1007/s40964-024-00646-5.
40. Hu, F., Mikolajczyk, T., Pimenov, D. Y. and Gupta, M. K., Extrusion-Based 3D Printing of Ceramic Pastes: Mathematical Modeling and In Situ Shaping Retention Approach, *Materials (Basel)*, Vol. 14, 1137, 2021, https://doi.org/10.3390/ma14051137.
41. ASTM International, ASTM D790-17, Standard Test Methods for Flexural Properties of Unreinforced and Reinforced Plastics and Electrical Insulating Materials, PA, USA, 2017, https://www.universalgripco.com/astm-d790, [Accessed: Oct. 5, 2025].
42. International Organization for Standardization, Coating powders: Determination of psize distribution by sieving, ISO 8130-1:2019, Apr. 2019, https://www.iso.org/standard/68393.html, [Accessed: Aug. 10, 2025].
43. Insua, I., Etzold, O., Calafel, I., Aguirresarobe, R., Calderón, M. and Fernández, M., Rheological Insight into the 3D Printability of Carboxymethyl Cellulose-Based Hydrogels, *Gels*, Vol. 11, 259, 2025, https://doi.org/10.3390/gels11040259.

Paper submitted: 31.01.2026
Paper revised: 08.04.2026
Paper accepted: 17.04.2026